THE JOURNAL OF PHYSICAL CHEMISTRY B

Article

Cite This: J. Phys. Chem. B 2019, 123, 4193−4203

pubs.acs.org/JPCB

Polyglutamine Solution-State Structural Propensity Is Repeat Length Dependent

Ryan S. Jakubek,[†] Riley J. Workman,[§,∥] Stephen E. White,[†,‡] and Sanford A. Asher*[,†]

[†]Department of Chemistry and [‡]Molecular Biophysics and Structural Biology Program, University of Pittsburgh, Pittsburgh, Pennsylvania 15260, United States

[§]Department of Chemistry and Biochemistry, Center for Computational Sciences, Duquesne University, Pittsburgh, Pennsylvania 15282, United States

Supporting Information

ABSTRACT: Expanded polyglutamine (polyQ) tracts in proteins, which are known to induce their aggregation, are associated with numerous neurodegenerative diseases. Longer polyQ tracts correlate with faster protein aggregation kinetics and a decreased age of onset for polyQ disease symptoms. Here, we use UV resonance Raman spectroscopy, circular dichroism spectroscopy, and metadynamics simulations to investigate the solution-state structures of the $D_2Q_{15}K_2$ (Q15) and $D_2Q_{20}K_2$ (Q20) peptides. Using metadynamics, we explore the conformational energy landscapes of Q15 and Q20 and investigate the relative energies and activation barriers between these low-energy structures. We compare the solution-state structures of $D_2Q_{10}K_2$ (Q10), Q15, and Q20 to determine the dependence of polyQ structure on the Q tract length. We show that these peptides can adopt two distinct monomeric conformations: an aggregation-resistant PPII-like conformation and an aggregation-prone β-strand-like conformation. We find that longer polyQ peptides have an increased preference for the aggregation-prone β-strand-like conformation. This preference may play an important role in the increased aggregation rate of longer polyQ peptides that is thought to lead to decreased neurodegenerative disease age of onset for polyQ disease patients.

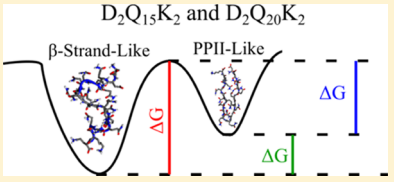

INTRODUCTION

The expansion of CAG codon repeats in DNA encodes for elongated polyglutamine (polyQ) tracts in proteins.[1] Expanded polyQ tracts in proteins and peptides induce aggregation and fibrillization. This aggregation is associated with numerous neurodegenerative diseases, including Huntington's disease.[1] However, the identity of the toxic species is still debated.[2−5]

For polyQ diseases, the length of the expanded polyQ tract affects the severity of the disease. Patients with longer polyQ tracts have an earlier disease age of onset, and disease symptoms are only evident if the protein's polyQ tract surpasses a critical length.[6−8] For example, clinical presentation of Huntington's disease is only observed in patients with a polyQ tract of ≥36 residues long in the huntingtin protein.[1] Additionally, in vitro studies of polyQ peptides show that longer polyQ tracts have increased aggregation rates that may be related to the disease age of onset.[6,9]

Because of the dependence of aggregation rate and disease age of onset on the length of the polyQ tract, there is great interest in determining the structural differences between polyQ tracts of different lengths. Most experimental[10−13] and computational[14−17] studies conclude that solution-state polyQ peptides are intrinsically disordered regardless of the polyQ tract length. However, some studies suggest the existence of small populations of secondary structure that may play a role in aggregation and cytotoxicity.[6,10,11]

UV resonance Raman (UVRR) spectroscopy has provided detailed insight into the secondary structures of polyQ peptides.[20−22] UVRR spectroscopy is a powerful tool for studying protein structure, solvation, and hydrogen bonding interactions.[23−25] Excitation in the deep UV (~200 nm) selectively enhances vibrations of the secondary amide peptide backbone and primary amide glutamine (Gln) side chains.[26,27] These resonance-enhanced bands are sensitive to the structure and environment of the peptide backbone and Gln side chains.[24]

Recently, Punihaole et al. used UVRR spectroscopy and metadynamics simulations to investigate the solution-state structures of $D_2Q_{10}K_2$ (Q10).[20] They found that when Q10 is dissolved in water it exists in a well-defined, collapsed β-strand-like conformation. This peptide form is referred to as non-disaggregated Q10 (NDQ10). In contrast, when disaggregated using the methodologies of Chen et al.,[28] Q10 exists in a predominantly polyproline II (PPII)-like structure. This peptide conformation is referred to as disaggregated Q10 (DQ10). NDQ10 and DQ10 were found to have a large activation barrier, preventing these two conformations from interconverting.[20] Disaggregated peptides, including DQ10, are more resistant to aggregation and fibrillization compared to non-disaggregated peptides.[21,27,28]

In this study, we use UVRR spectroscopy, circular dichroism (CD), and metadynamics simulations to investigate the solution-state structures of $D_2Q_{15}K_2$ (Q15) and $D_2Q_{20}K_2$

Received: February 13, 2019
Revised: April 17, 2019
Published: April 22, 2019

DOI: 10.1021/acs.jpcb.9b01433
J. Phys. Chem. B 2019, 123, 4193−4203

(Q20) in their disaggregated (D) and non-disaggregated (ND) forms. We compare our results with those previously published for Q10[20] and Q20[22] to investigate the dependence of the solution-state polyQ structures on repeat length. We find that disaggregated Q15 (DQ15) has predominately the same PPII-like structure as previously found for DQ10[20] and disaggregated Q20 (DQ20).[22] Also, non-disaggregated Q15 (NDQ15) has predominately the same collapsed β-strand-like conformation as previously found for NDQ10.[20] Unlike NDQ10 and NDQ15, non-disaggregated Q20 (NDQ20) is insoluble in water. The structures of NDQ20 were previously described in detail.[22]

Using CD spectroscopy, we show that disaggregated polyQ (DQ) peptides, while predominantly in a PPII-like conformation, have a significant population of collapsed β-strand-like conformation that increases with polyQ length. Our metadynamics simulations show that the relative energies of the PPII-like structures increase and the relative activation energy of the PPII $\rightarrow$ β-strand conformational transition decreases with increasing polyQ length. From these data, we conclude that longer polyQ peptides have an increased preference for the aggregation-prone collapsed β-strand-like conformation compared to the aggregation-resistant PPII-like conformation. This structural preference may in part explain why proteins containing longer polyQ tracts have an increased aggregation rate, which is associated with a decrease in the neurodegenerative disease age of onset.

MATERIALS AND METHODS

Materials. The peptides Q15 and Q20 were purchased from Thermo Fisher Scientific at ≥95% purity. Trifluoroacetic acid (TFA) was purchased from Thermo Fisher Scientific at ≥99.5% purity, and 1,1,1,3,3,3,-hexafluoro-2-propanol (HFIP) was purchased from Acros Organics at ∼99% purity.

Sample Preparation. NDQ15 was prepared by dissolving the peptide in nanopure water. Solution-state, non-disaggregated polyQ peptides are sensitive to impurities that can nucleate aggregation. NDQ15 was prepared in sterile centrifuge tubes to remove any nucleating centers.

DQ15 and DQ20 were prepared using the disaggregation protocol developed by Chen et al.[28] Briefly, the peptide was dissolved in 1:1 TFA/HFIP by sonication (∼15 min) and incubated for ∼2 h at room temperature. The TFA/HFIP solvent was then evaporated with a stream of dry nitrogen, and the peptide was dissolved in water to the desired concentration (0.3 mg/mL for UVRR and CD measurements).

UV Resonance Raman Spectroscopy. The UVRR instrumentation used in this work was previously described by Bykov et al.[29] An Infinity Nd:YAG laser (Coherent, Inc.) was used to generate ∼204 nm light by Raman-shifting the third harmonic with H_2 gas (30 psi) and using the fifth anti-Stokes line. We generated 197 nm laser excitation using the fourth harmonic of a tunable Ti:sapphire laser (Positive Light). Samples were contained in a spinning Suprasil quartz NMR tube during spectral collection, and a ∼165° backscattering angle was used. The scattered light was dispersed in a subtractive double monochromator. A back-thinned, liquid nitrogen-cooled CCD camera (Spec10:400B, Princeton Instruments) with a Lumagen-E coating was used to detect the Raman scattering.

CD Spectroscopy. CD spectra were measured using a Jasco J-710 spectropolarimeter. Samples were placed in a cylindrical fused silica quartz cuvette with a pathlength of 0.02 cm. Spectra were collected with 0.2 nm data intervals and averaged over ∼10 scans.

Computational Methods. *General Simulation Details.* Metadynamics simulations were used to investigate the conformational energy landscape of Q15 and Q20. Subsequently, molecular dynamics (MD) simulations were performed on low-energy conformations of the Q15 and Q20 landscapes to obtain structural information on the equilibrated structures. Monomeric Q15 and Q20 peptides were placed in periodic boxes of 11665 and 18658 TIP3P[30] water molecules with dimensions of 72 × 72 × 72 Å and 84 × 84 × 84 Å, respectively. All simulations were performed with the NAMD[31] MD engine, and simulation trajectory data were analyzed using Visual Molecular Dynamics (VMD) 1.9.2[32] with a Tcl scripting interface.

Potential energies were calculated using the CHARMM36 force field.[33] The particle mesh Ewald algorithm[34] (1.0 Å grid spacing) was used to calculate system electrostatics. An integration time step of 2 fs was used. The NPT ensemble (constant atom number, pressure, temperature) was used for all simulations with a Langevin thermostat and piston to maintain temperature and pressure at 300 K and 1.01225 bar, respectively.[35] The pair list distance, interaction cutoff, and switch distance were 14.0, 12.0, and 10.0 Å, respectively.

Metadynamics Simulations. Well-tempered metadynamics simulations were used to characterize the conformational free energy landscape of the Q15 and Q20 peptides. Metadynamics is a method that enhances the sampling of a standard MD simulation by adding artificial potentials, in the form of Gaussian functions, to conformations that the system previously sampled. This allows the system to escape deep energy wells and to sample a large region of its conformational energy landscape.[36,37]

The initial Q15 and Q20 peptide monomers used in the metadynamics simulations were fully extended peptides with Ramachandran Φ and Ψ angles of 180°. The peptide systems were energy-minimized for 10 000 steps, using the conjugate gradient method, and then equilibrated for 500 ps. Metadynamics was then performed on the equilibrated system for 400 ns of simulation time.

To visualize the Q15 and Q20 conformational landscapes, we plotted the metadynamic conformations using the root-mean-square deviation (RMSD) for the α-carbon positions of idealized α-helix, β-hairpin, and PPII conformations of Q15 or Q20. These collective variables are similar to that previously used by Punihaole et al.[20] Ideal α-helix, β-hairpin, and PPII collective variable reference structures were created with Molecular Operating Environment[38] software (MOE 2013.10). The maximum RMSDs for metadynamics structures were set to 15 and 20 Å for Q15 and Q20 respectively, and this limit was maintained by a 1.0 kcal mol^{-1} Å^{-1} half-harmonic potential constraint. Artificial potentials, in the form of Gaussian functions with a height of 1.0 kcal mol^{-1} and a width of 0.3 Å for Q15 and 0.4 Å for Q20, were added to the metadynamics simulations every 100 steps. The metadynamics free energy data and collective variable history were processed using Python scripts to identify the landscape positions and structures for conformations found in local energy wells. The scripts and coordinate files used in the metadynamics simulations are provided in the Supporting Information.

Metadynamics simulation parameters were chosen to minimize error and ensure adequate sampling of the energy landscape following the work of Laio et al.[39] Also, Laio et al.[39] empirically derived an equation to estimate the error of metadynamics simulations for systems with energy landscapes

DOI: 10.1021/acs.jpcb.9b01433
J. Phys. Chem. B 2019, 123, 4193−4203

containing only a few well-defined energy wells. However, our system contains complex energy landscapes with many local energy minima. Thus, the methods developed by Laio et al.[39] are unable to estimate the error in our simulations.

MD simulations (10 ns) were used to obtain equilibrium structural information on the low-energy conformations found in the metadynamics energy landscapes. Ψ and Φ dihedral angles were extracted from simulation trajectories using a Tcl script in VMD.

RESULTS AND DISCUSSION

UVRR Spectroscopy. UVRR spectroscopy, with a ∼204 nm excitation wavelength, is in resonance with the $\pi \rightarrow \pi^*$ transitions of amide groups, including the secondary amides of the peptide backbone[26] and the primary amides of the Gln side chains.[27,40,41] Therefore, the UVRR spectra of our polyQ peptides are dominated by the resonance-enhanced vibrations located on these amide chromophores. This greatly simplifies the vibrational spectrum of these peptides.

As discussed above, Punihaole et al. previously showed that NDQ10 exists in a β-strand-like conformation, while DQ10 is in a PPII-like conformation.[20] Also, Jakubek et al. previously showed that DQ20 is also in a PPII-like conformation.[22] Here, we used UVRR to investigate the structures of solution-state NDQ15 and DQ15.

We previously discussed detailed UVRR band assignments for NDQ10,[20] DQ10,[20] NDQ20,[22] and DQ20.[22] Here, we find that the UVRR spectra and band assignments of NDQ15 are essentially identical to those of NDQ10.[20] Also, we find that the UVRR spectra and band assignments of DQ15 are essentially identical to those of DQ10[20] and DQ20[22] (Figure 1). As such, we will only discuss the assignment of the conformationally sensitive amide III_3 band of the peptide backbone ($AmIII_3^S$). A complete discussion of assignments can be found in the previous work by Punihaole et al.[20]

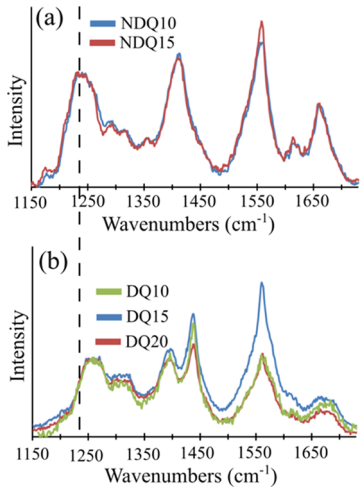

Figure 1. UVRR spectra (204 nm) of solution-state polyQ peptides: (a) NDQ10 and NDQ15; (b) DQ10, DQ15, and DQ20. All spectra were normalized to the $AmIII_3^S$ band. The dashed line is located at ∼1240 cm^{-1}. The UVRR spectra of NDQ10 and DQ10 were previously reported by Punihaole et al.,[20] and the UVRR spectrum of DQ20 was previously reported by Jakubek et al.[22] NDQ10 and DQ10 spectra were adapted with permission from Punihaole, D. et al. (2016) J. Phys. Chem. B. 120(12), 3012−3026. Copyright 2016 American Chemical Society. DQ20 spectra were adapted with permission from Jakubek, R. et al. (2019) J. Phys. Chem. B., 123 (8), 1749−1763. Copyright 2019 American Chemical Society.

Ramachandran Ψ Angle Distributions of Q15 and Q20. Asher et al. previously showed that the frequency of the $AmIII_3^S$ band sinusoidally depends on the Ramachandran Ψ angle of the peptide backbone.[42] This correlation results from the coupling of the backbone N−H bending motion of the $AmIII_3^S$ band with the $C_\alpha H$ bending vibration at ∼1390 cm^{-1}.[42] Mikhonin et al. later developed a method to quantitatively calculate the Ramachandran Ψ angle of a peptide backbone in a variety of different solvation states and sample temperatures.[43]

Asher et al. showed that the Ψ angle distribution of a peptide can be estimated from the inhomogeneous line width of the $AmIII_3^S$ band.[44] Assuming that the inhomogeneous broadening is solely due to the Ψ angle distribution of the peptide, one can model the $AmIII_3^S$ band as a sum of Lorentzian bands with a width equal to the homogeneous linewidth of the $AmIII_3^S$ band. Using the equations derived by Mikhonin et al.,[43] the corresponding Ψ angle can be calculated for each Lorentzian band producing a Ψ angle distribution. These methodologies have previously been used to estimate the Ψ angle distribution in a variety of peptides,[25,45,46] including those of polyQ.[20−22,27]

Here, we use these methods to calculate the Ψ angle distributions of NDQ15 and DQ15 (Figure 2a−c) from the UVRR spectral fits (Figure 3). The UVRR spectrum of NDQ15 contains an $AmIII_3^S$ band centered at ∼1240 cm^{-1}. This corresponds to a Ψ angle distribution that peaks at Ψ ∼140°, which is consistent with β-strand conformations.[47] The $AmIII_3^S$ band and Ψ angle distribution of NDQ15 are essentially identical to those of NDQ10.[20] Thus, we conclude that the secondary structure of NDQ15 is the same as that of the NDQ10 collapsed β-strand-like conformation.[20]

DQ15 contains $AmIII_3^S$ bands at ∼1275, ∼1250, and ∼1215 cm^{-1}, which correspond to Ψ angle distributions peaked at ∼175, ∼150, and ∼10°, respectively. Ramachandran Ψ angles of ∼175, ∼150, and ∼10° are characteristic of 2.5_1-helix, PPII-helix, and turn-like structures, respectively.[43] The $AmIII_3^S$ bands and Ψ angle distribution of DQ15 are the same as those previously observed for DQ10[20] and DQ20.[22] Thus, we conclude that the secondary structure of DQ15 is the same as that of DQ10/DQ20.[20] From UVRR and metadynamics simulations, DQ10 was previously found to be in a PPII-helix-like conformation interspersed with turn-like structures and with a subpopulation of 2.5_1-helix conformation localized on the charged terminal residues.[20] Additional information regarding our Ψ angle distribution calculations and spectral fitting can be found in the Supporting Information.

Assuming equal Raman cross sections, we roughly estimate the relative fraction of each secondary structure found in DQ10, DQ15, and DQ20 from the $AmIII_3^S$ band areas. We find that DQ10, DQ15, and DQ20 contain roughly ∼55% PPII-like, ∼30% turn-like, and ∼15% 2.5_1-helix-like conformations. 2.5_1-helix-like conformation (15%) corresponds to ∼2−3 peptide bonds per peptide.

Punihaole et al.[20] previously showed that the 2.5_1-helix structure of DQ10 is localized on the charged terminal residues. This is because the 2.5_1-helix conformation derives primarily from the electrostatic repulsions of adjacent, charged amino acids.[48,49] Our observation that DQ10, DQ15, and DQ20 contain ∼2−3 peptide bonds in the 2.5_1-helix conformation is consistent with the localization of the 2.5_1-helix on the charged terminal residues.

DOI: 10.1021/acs.jpcb.9b01433
J. Phys. Chem. B 2019, 123, 4193−4203

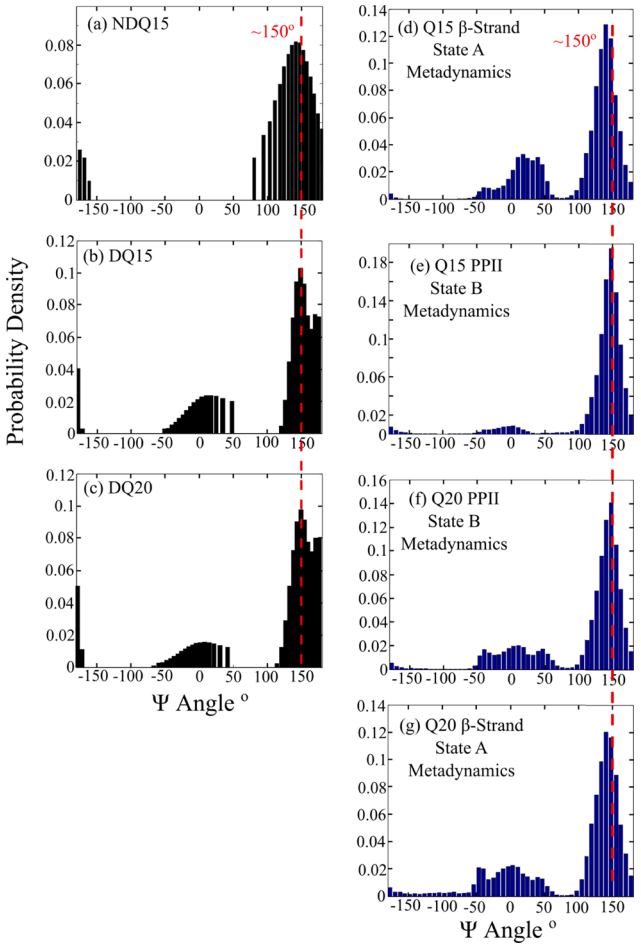

Figure 2. Experimental Ψ angle distributions of solution-state (a) NDQ15, (b) DQ15, and (c) DQ20. Computational Ψ angle distributions from metadynamics energy wells for (d) Q15 state A, (e) Q15 state B, (f) Q20 state B, and (g) Q20 state A. The experimental and computational Ψ angle distributions of NDQ10 and DQ10 can be found in ref 20. The experimental Ψ angle distribution for DQ20 was previously reported by Jakubek et al.[22] The experimental DQ20 Ψ distribution was adapted with permission from Jakubek, R. et al. (2019) J. Phys. Chem. B. 123 (8), 1749−1763. Copyright 2019 American Chemical Society.

Metadynamics Structures of Q15 and Q20. To obtain further insights into the solution-state structures of Q15 and Q20, we performed metadynamics simulations to investigate their conformational energy landscapes. The use of metadynamics to examine the polyQ energy landscape was previously demonstrated by Punihaole et al.[20] The metadynamics conformational landscapes of Q15 and Q20 are found in Figure 4. As previously observed for Q10, the energy landscapes for Q15 and Q20 are frustrated with many shallow local minima. For both Q15 and Q20, we find two deep, local energy wells on the energy landscape that correspond to different low-energy structures. We will designate these conformations as state A and state B. Representative structures from each energy well are shown in Figure 4. We examine the Φ and Ψ angle distributions of conformations found in state A and state B for both Q15 and Q20 (Figure 5). The state A and state B conformations are similar for both Q15 and Q20.

State A of Q15 and Q20 both contain peptide bonds with (Φ, Ψ) angle populations of (−95, 140°) and (−65, 140°), which are found in the β-sheet region of the Ramachandran plot.[47]

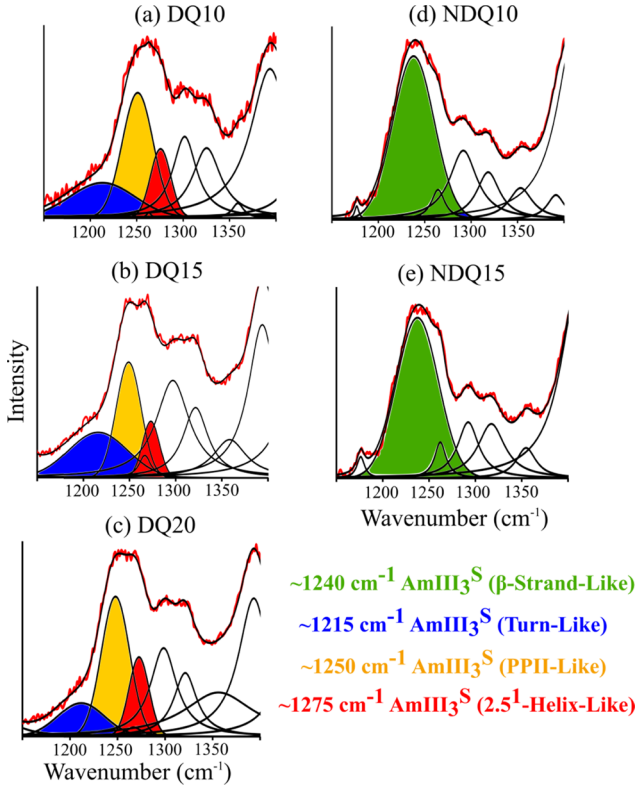

Figure 3. Spectral fits for the $AmIII_3^S$ UVRR spectral regions of (a) DQ10, (b) DQ15, (c) DQ20, (d) NDQ10, and (e) NDQ15. The $AmIII_3^S$ bands are color-coded as described in the figure legend. NDQ10 and DQ10 spectra were adapted with permission from Punihaole, D. et al. (2016) J. Phys. Chem. B. 120(12), 3012−3026. Copyright 2016 American Chemical Society. DQ20 spectra were adapted with permission from Jakubek, R. et al. (2019) J. Phys. Chem. B. 123 (8), 1749−1763. Copyright 2019 American Chemical Society.

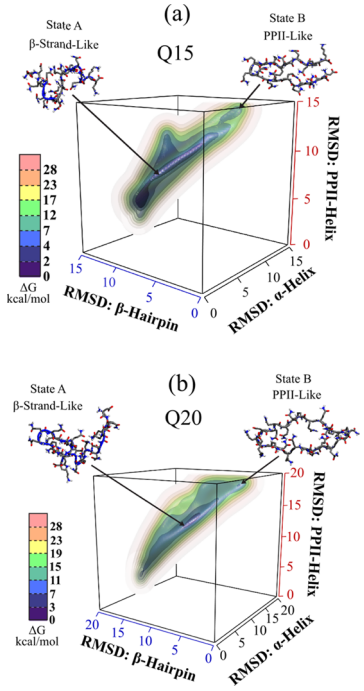

Figure 4. Conformational energy landscapes of (a) Q15 and (b) Q20 obtained from metadynamics simulations.

DOI: 10.1021/acs.jpcb.9b01433
J. Phys. Chem. B 2019, 123, 4193−4203

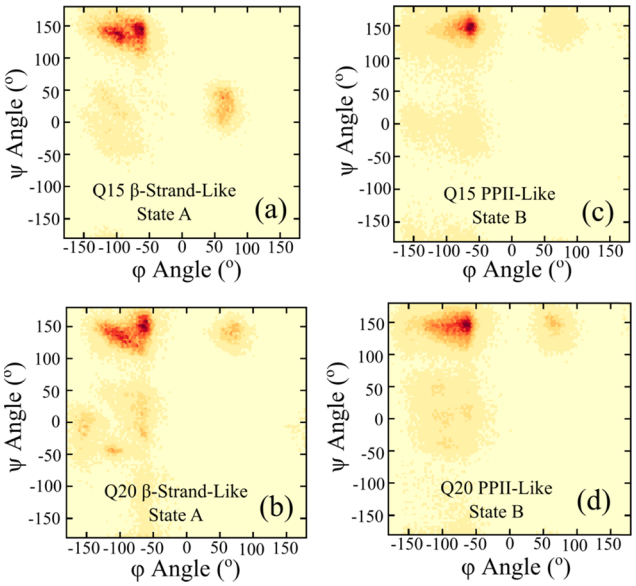

Figure 5. Ramachandran plots for (a) Q15 state A, (b) Q20 state A, (c) Q15 state B, and (d) Q20 state B metadynamics structures. Darker red colors indicate an increased number of peptide bonds in a given region of the Ramachandran plot.

Also, the structures of state A contain a broad Ψ angle distribution centered at ∼0°, which is characteristic of turn-like structures.[47] The Ψ angle distributions of the state A structures for Q15 and Q20 are centered at ∼140°. This Ψ angle distribution is in quantitative agreement with that observed for NDQ15. Thus, we conclude that state A of the metadynamics landscape corresponds to the structure of the non-disaggregated peptide. The structure and (Φ, Ψ) distributions of state A for Q15 and Q20 are similar to the state A metadynamics structure of Q10 previously reported.[20] From our metadynamics simulations, we conclude that state A consists of a predominately β-strand-like secondary structure with turn-like structural regions that allow the structure to be collapsed.

For state B structures of Q15 and Q20, we find that the (Φ, Ψ) angle distribution peaks at (−65, 150°). These angles are found in the PPII region of the Ramachandran plot.[50] We also find a significant population of Ψ angles centered at ∼0° (see Figure 2), which is characteristic of turn-like conformations.[47] The Ψ angle distribution of state B is centered at ∼140° (see Figure 2). This Ψ angle distribution is in quantitative agreement with those observed for DQ15 and DQ20 (Figure 2). Thus, we conclude that state B of the metadynamics landscape corresponds to the structures of DQ15 and DQ20. The structure and (Φ, Ψ) distributions of state B for Q15 and Q20 are similar to the state B metadynamics structure of Q10 previously reported.[20] From our metadynamics simulations, we conclude that state B consists of predominately PPII-like secondary structures with turn-like structures enabling the structure to be collapsed.

In the experimental Ψ angle distributions calculated from UVRR spectra of DQ10−20, we find a peak at ∼175°, which we assign to 2.5_1-helix conformations. However, we do not observe this peak in the state B metadynamics structure. As discussed previously by Punihaole et al.[20] and Feng,[51] this discrepancy likely results from an inadequacy in the CHARMM36 force field. The CHARMM36 force field was optimized using X-ray crystal structures of proteins.[52] The 2.5_1-helix is an uncommon structure that is found only in peptide sequences with adjacent, charged amino acids.[48] Thus, it is unlikely that this structure is well parameterized in the CHARMM36 force field.

For Q15 and Q20, the β-strand-like energy well (state A) in the metadynamics simulations is conformationally broad. As a result, the metadynamics β-strand-like structure can vary with a low free energy cost. This suggests that the β-strand-like structure is flexible with significant conformational variability. In contrast, the PPII-like energy well (state B) of Q15 and Q20 is narrow, indicating a more well-defined structure with less structural variability.

In contrast, metadynamics simulations of Q10 have revealed narrow energy distributions for both the PPII-like and β-strand-like structures.[20] Our observation that the Q10 peptide contains less conformational variability compared to Q15 and Q20 is in agreement with the computational work of Wang et al.[17] They used molecular dynamics simulations to investigate the structures of Q5 and Q15 peptides. In contrast to this study, their results indicate that both Q5 and Q15 are disordered in solution. However, they find that Q15 has increased conformational variability compared to Q5. This is thought to result from an increase in the number of possible peptide−peptide hydrogen bonding contacts with longer polyQ tracts. They conclude that longer polyQ peptides have increased aggregation kinetics because their conformational variability allows the peptide to sample β-sheet structures that nucleate fibrillization.[17]

Overall, our metadynamics simulations agree with our UVRR data showing that the structure of NDQ15 is predominately a β-strand-like conformation, while the structure of DQ15 and DQ20 is predominantly a PPII-like conformation. This result is similar to that previously reported for DQ10 and NDQ10.[20]

Circular Dichroism Spectroscopy of Q15 and Q20. *CD Spectra of DQ15, DQ20, and NDQ15.* To further investigate the structures of Q15 and Q20, we collected CD spectra of NDQ15, DQ15, and DQ20 (Figure 6). The CD spectrum of

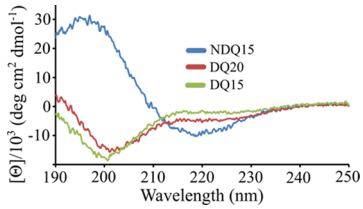

Figure 6. CD spectra of NDQ15 (blue), DQ15 (green), and DQ20 (red).

NDQ15 consists of a negative peak at ∼218 nm and a strong positive peak at ∼196 nm, which is characteristic of β-sheet conformations.[53] In contrast, the spectra of both DQ15 and DQ20 have strong negative peaks at ∼200−205 nm that are characteristic of PPII conformations.[53] Our CD spectra are consistent with our UVRR measurements and metadynamics simulations, concluding that our DQ peptides are in a PPII-like conformation and our NDQ peptides are in a β-strand-like conformation.

DQ20 and DQ15 Have a Population of β-Strand Structures. We compared the CD spectra of DQ15, DQ20, and DQ10 (Figure 7a). The CD spectrum of DQ10 was previously measured by Punihaole et al.[20] Both the DQ20 and DQ15 spectra show a less negative and slightly red-shifted peak at ∼200−205 nm and a more positive peak at ∼190 nm compared to DQ10. Also, the trough at ∼220 nm is more negative for DQ20 compared to that for DQ10. To highlight the

DOI: 10.1021/acs.jpcb.9b01433
J. Phys. Chem. B 2019, 123, 4193−4203

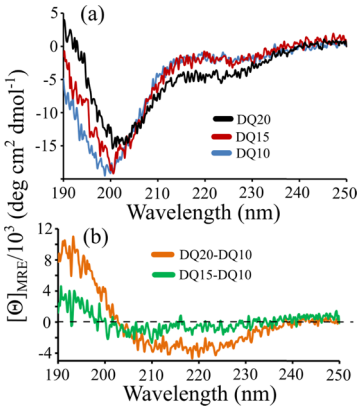

Figure 7. Comparison of DQ10−20 CD spectra. (a) CD spectra of (blue) DQ10, (red) DQ15, and (black) DQ20. (b) CD difference spectra of (orange) DQ20−DQ10 and (green) DQ15−DQ10. DQ10 CD spectra were adapted with permission from Punihaole, D. et al. (2016) J. Phys. Chem. B. 120(12), 3012−3026. Copyright 2016 American Chemical Society.

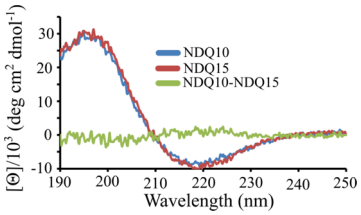

Figure 8. CD spectra of (blue) NDQ10, (red) NDQ15, and (green) NDQ10−NDQ15 difference spectrum. NDQ10 CD spectra were adapted with permission from Punihaole, D. et al. (2016) J. Phys. Chem. B. 120(12), 3012−3026. Copyright 2016 American Chemical Society.

spectral differences, we subtracted the DQ10 spectrum from that of DQ20 and DQ15 (Figure 7b). The difference spectra contain a negative weak peak at ∼220 nm and a stronger positive peak at ∼195 nm. This is characteristic of β-sheet conformations[53] and is similar to the CD spectra of NDQ10 and NDQ15.

We modeled the spectra of DQ15 and DQ20 as a linear combination of DQ10 and NDQ15 basis spectra. We chose these basis spectra because these peptides best represent the pure β-strand-like and PPII-like conformations of polyQ, respectively (see the Supporting Information for details). The spectra of DQ15 and DQ20 are well modeled using NDQ15 and DQ10 CD spectra as basis spectra (Figures S1 and S2). This suggests that the CD spectral differences between DQ10, DQ15, and DQ20 result from differing amounts of a minority β-strand-like population in the DQ peptides. We used our model to estimate the percentage of collapsed β-strand-like structures in DQ15 and DQ20 (see the Supporting Information). We find that DQ15 and DQ20 contain ∼5 and ∼15% β-strand conformations, respectively. These data show that, at least for Q10−Q20, longer DQ peptides contain an increasing population of the β-strand-like structure.

Our result is in great agreement with that reported by Chellgren et al. who examined the CD spectra of disaggregated polyQ peptides containing 1−15 Gln residues.[18] They find that the negative peak at ∼205 nm decreases in magnitude and the positive peak at ∼225 nm increases in magnitude with increasing polyQ tract length, which is similar to what we observe for DQ10−20. From their CD data, Chellgren et al. conclude that longer DQ peptides have decreased PPII content and increased β-strand/sheet content.[18] They report that their DQ15 peptide has ∼7% β-strand population, which is similar to what we observe for DQ15.

We also compared the CD spectra of NDQ15 and NDQ10 (Figure 8). The CD spectrum of NDQ10 was previously measured by Punihaole et al.[20] We find that the CD spectra of NDQ10 and NDQ15 are essentially identical. This indicates that the NDQ10 and NDQ15 peptides do not have a structural dependence on polyQ length.

Detectivity of UVRR Spectroscopy to Minority PPII-Like and β-Strand-Like Populations. Our CD measurements show that DQ15 and DQ20 contain minority populations of β-strand-like structures. However, these subpopulations are not clearly observed in our UVRR spectra. One possible origin for this discrepancy is that the UVRR spectra may not be adequately sensitive to the small subpopulation of β-strand-like secondary structures in the presence of a dominantly PPII-like conformation.

We examined the sensitivity of 204 nm excited UVRR spectroscopy to detect β-strand-like subpopulations in DQ peptides by artificially adding a β-strand-like $AmIII_3^S$ peak (1240, 40 cm^{-1} FWHH) to the spectral fit of DQ20. The area of the 1250 cm^{-1} PPII-like $AmIII_3^S$ band was reduced to conserve the total $AmIII_3^S$ band area. This spectrally models an increase in the β-strand-like population in the presence of a corresponding decrease in the PPII-like conformation, assuming equal Raman cross sections.

We qualitatively compared the UVRR spectrum of DQ20 to spectral fits that model 10, 20, 30, 50, and 80% β-strand-like minority populations. We find that the spectral fit does not significantly differ from that of the DQ20 spectrum until the β-strand subpopulation exceeds ∼20%. We conclude that the UVRR spectra have low sensitivity to β-strand-like subpopulations because the 1240 cm^{-1} β-strand-like $AmIII_3^S$ band is broad (40 cm^{-1} FWHH) and overlaps more intense bands in the $AmIII_3^S$ spectral region. Our result suggests that the UVRR limit of detection for β-strand subpopulations is ∼ ≥20%.

Gibbs Free Energies and Activation Energies for PolyQ Metadynamics Structures. The Gibbs free energies and activation barriers for the metadynamics polyQ structures are summarized in Figure 9.

Gibbs Free Energies of the β-Strand-Like and PPII-Like Metadynamics Structures. Table 1 shows the difference in the Gibbs free energy of the β-strand-like and the PPII-like conformations calculated for Q10, Q15, and Q20 using metadynamics. The β-strand-like conformation is found at the global energy minimum of the landscape for Q10, Q15, and Q20. We find that the difference in the Gibbs free energy between the PPII-like and β-strand-like conformations increases as the polyQ tract length increases. From this result, we conclude that the PPII-like conformation is less energetically favorable, compared to the β-strand-like conformation, for longer polyQ peptides.

Activation Barriers between PPII and β-Strand Conformations. Using metadynamics, we calculated the activation barriers for the PPII-like → β-strand-like and β-strand-like → PPII-like conformational transitions of Q10−20. As stated above, the energy landscapes of Q10−20 are rough with many local minima. Thus, the activation barrier for interconversion between structures heavily depends on the pathway the peptide takes through its conformational landscape.

DOI: 10.1021/acs.jpcb.9b01433
J. Phys. Chem. B 2019, 123, 4193−4203

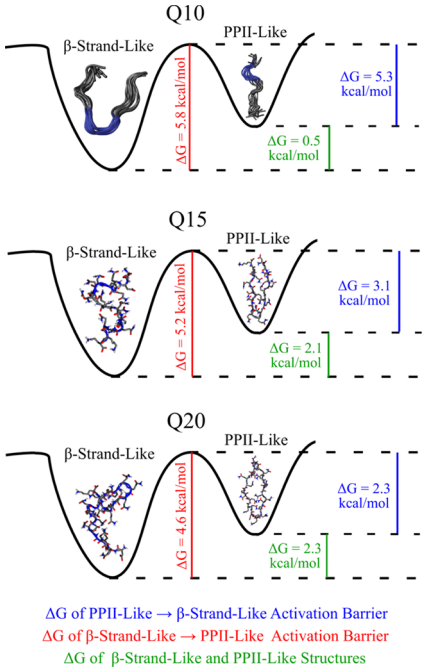

Figure 9. Depiction of relative energies and activation barriers for the Q10−20 PPII-like and β-strand-like conformations. The activation barrier ΔG for the β-strand → PPII transitions is shown in red, the activation barrier ΔG for the PPII → β-strand transitions is shown in blue, and the relative ΔG of the β-strand-like and PPII-like minima is shown in green. Molecular models of Q10 were adapted with permission from Punihaole, D. et al. (2016) J. Phys. Chem. B. 120(12), 3012−3026. Copyright 2016 American Chemical Society.

Table 1. Difference in the Gibbs Free Energies of the β-Strand-Like and PPII-Like Conformations of Q10, Q15, and Q20

	(ΔG PPII)-(ΔG β-strand) (kcal/mol)
Q10	0.5
Q15	2.1
Q20	2.3

We calculated the lowest energy activation barriers for the PPII-like → β-strand-like and β-strand-like → PPII-like structural conversions from the metadynamics free energy landscapes. The lowest energy pathway between the PPII-like and β-strand-like energy wells was identified using a Monte Carlo method, where random pathways were sampled and their activation barriers minimized. The lowest activation barrier between the PPII-like and β-strand-like states was identified, as the Monte Carlo simulations converged upon a pathway with minimum activation energy. The values reported in Table 2 are those of the lowest energy pathways for the respective structural conversion.

From the metadynamics simulations, we find that the PPII → β-strand activation barriers are lower compared to the β-strand → PPII activation barriers for Q10, Q15, and Q20. We observe a decrease in both the β-strand → PPII and PPII → β-strand energy barriers with increasing peptide length. Also, we examined the energy difference between the β-strand → PPII and PPII → β-strand activation barriers. We find that the PPII → β-strand activation barrier decreases relative to the β-strand → PPII activation energy with increasing polyQ length.

Our metadynamics results for the relative energies and activation energies of Q15 and Q20 indicate that longer polyQ peptides increasingly prefer the β-strand-like conformation. This is in agreement with our CD data showing that, for DQ10−20, longer polyQ peptides have an increased population of β-strand-like conformation. Overall, these data show that the aggregation-prone β-strand-like conformation is increasingly preferred for longer polyQ peptides.

It is possible that increased hydrogen bonding contacts for larger polyQ peptides stabilize the β-strand-like structure over the PPII-like structure. Walters et al.[54] used fluorescence resonance energy transfer (FRET) to show that longer polyQ peptides are more collapsed. They hypothesized that longer polyQ peptides have increased possible peptide−peptide hydrogen bonding contacts, resulting in an unordered collapsed structure.[54] PPII structures are stabilized by water−peptide interactions,[55−59] while β-strand structures are stabilized by peptide−peptide hydrogen bonding.[22,60] Therefore, we hypothesize that longer polyQ peptides may have increased hydrogen bonding contacts that stabilize the β-strand-like conformation over the PPII-like conformation.

In addition, Walters et al.[54] hypothesized that the increased number of possible peptide−peptide hydrogen bonding contacts for longer polyQ peptides increases the probability of their formation. Jakubek et al.[22] previously proposed that the PPII → β-strand activation energy is associated with the disruption of peptide−water interactions while forming intrapeptide hydrogen bonds. Thus, it is possible that the increased probability of longer polyQ tracts forming intrapeptide hydrogen bonds results in a decreased PPII → β-strand activation energy.

Q15−20 Conformation and Aggregation Kinetics. Our CD results show that, for DQ10−20 peptides, longer polyQ peptides have an increased population of collapsed β-strand structure. Also, our metadynamics simulations show that the β-strand conformation is increasingly thermodynamically favored for longer polyQ peptides. These results are important because the disaggregated PPII-like conformation resists aggregation, while the non-disaggregated collapsed β-strand-like conformation readily aggregates.[21,27] Thus, the increase of collapsed β-strand population of longer DQ peptides may contribute to their increased aggregation kinetics.[9]

Our result is similar to that of Darnell et al. who used CD spectroscopy to examine the structure of polyQ peptides of different lengths.[61] They found that short polyQ peptides are found in a PPII-like conformation and that increasing the length of the polyQ tract decreases the PPII-like content and increases

Table 2. Activation Barrier Energies for the β-Strand-Like → PPII-Like and PPII-Like → β-Strand-Like Conformational Transitions in Q10, Q15, and Q20

	β-strand → PPII (kcal/mol)	PPII → β-strand (kcal/mol)	(β-strand → PPII)−(PPII → β-strand) (kcal/mol)
Q10	5.8	5.3	0.5
Q15	5.2	3.1	2.1
Q20	4.6	2.3	2.3

DOI: 10.1021/acs.jpcb.9b01433
J. Phys. Chem. B 2019, 123, 4193−4203

the β-sheet content of polyQ. From this, they conclude that polyQ peptides are in a "tug-of-war" between PPII and β-sheet structures where longer polyQ peptides prefer β-sheet structures, including fibrils. Our results provide further evidence that longer DQ peptides prefer β-strand structures.

Temperature Dependence of the NDQ15 and DQ20 CD Spectra. We also investigated the temperature dependence of the NDQ15 and DQ20 CD spectra (Figure 10). For NDQ15, we find that both the positive peak at ~195 nm and the negative peak at ~220 nm decrease in magnitude with increasing temperature. This spectral change is indicative of a decrease in the β-strand-like population of NDQ15 with increasing temperature. In agreement, the 20−50 °C difference spectrum shows a positive peak at ~195 nm and a negative peak at ~220 nm, which is characteristic of β-sheet conformations. Also, this decrease in β-strand-like conformation is reversible upon cooling the sample from 50 °C back to 20 °C (Figure 10a).

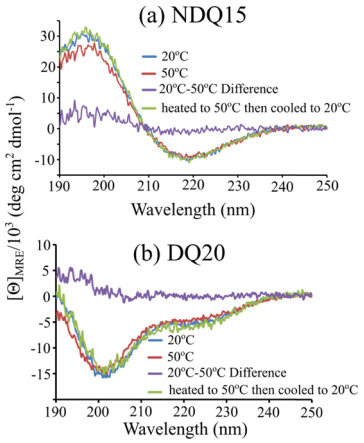

Figure 10. Temperature dependence of the (a) NDQ15 CD spectra and (b) DQ20 CD spectra. The blue spectra were collected at 20 °C, the red spectra were collected at 50 °C, and the purple spectra are the 20−50 °C difference spectra. The green spectra were collected after the sample was heated to 50 °C and cooled back down to 20 °C.

We find that the CD spectrum of DQ20 is also sensitive to temperature. Upon increasing the temperature of DQ20 from 20 to 50 °C, we observe a decrease in intensity at ~195 nm and a decrease in the trough at ~220 nm. These spectral changes are consistent with a decrease in the β-strand-like population of DQ20 with increasing temperature. The DQ20 20−50 °C difference spectrum shows a peak at ~195 nm, which is consistent with our conclusion that the lower-temperature DQ20 sample contains a larger population of β-strand-like structure (Figure 10b).

Our result is similar to that of Bhattacharyya et al. who reports the 5−35 °C difference spectrum of disaggregated $K_2Q_{40}K_2$ (Q40).[19] They find that the difference spectrum contains a moderate negative peak at ~220 nm, a very weak negative peak at ~205 nm, and a strong positive peak at ~195 nm. This is similar to the CD spectrum we observe for the β-strand-like NDQ10 and NDQ15 peptides. However, Bhattacharyya et al. conclude that this difference spectrum is characteristic of α-helices and that DQ40 forms α-helix conformations at low temperatures.[19]

Bhattacharyya et al. may conflate the β-strand signature of the 5−35 °C difference spectrum with that of an α-helix, which has a similar CD spectrum.[19] This may be in part due to the presence of a very weak negative peak at ~205 nm in their 5−35 °C difference spectra. The α-helix spectrum consists of a strong positive peak at ~190 nm, a moderate negative peak at ~208 nm, and a weak negative peak at ~222 nm.[53] Thus, the presence of a peak at ~205 nm may suggest α-helix conformation. However, this negative peak could also arise from the incomplete subtraction of the PPII structure, which has a strong negative peak at ~205 nm, in the 5−35 °C difference spectrum.

NDQ Conformational Flexibility May Contribute to Fast Aggregation Kinetics. As discussed above, we find that the β-strand-like energy wells in the metadynamics simulations are broad compared to the PPII-like energy wells for Q15 and Q20. Thus, the β-strand-like conformation can more easily sample different structures compared to the PPII-like conformation. This agrees with the temperature dependence of the NDQ15 and DQ20 CD spectra that, in both cases, show a decrease in β-strand population with increasing temperature.

In contrast, the metadynamics PPII-like energy wells are narrow, indicating that the PPII-like structure cannot easily sample different conformations. This is in agreement with the temperature dependence of the DQ20 CD spectrum that indicates no change in the PPII-like structure with increasing temperature. Also, the CD spectrum of DQ15 shows less temperature sensitivity compared to that of DQ20 (Figure S4). This is a result of DQ15 containing a smaller subpopulation of the temperature-sensitive β-strand-like conformation and a larger, temperature-insensitive PPII-like population.

Previously, Vitalis et al. and Wang et al. proposed that the conformational flexibility of polyQ peptides promotes their aggregation.[16,17] The flexibility of polyQ is thought to promote aggregation by increasing intermolecular interactions and/or increasing the probability of sampling β-sheet conformations that are prone to fibrillization. Both our metadynamics simulations and CD spectra show evidence that the β-strand-like conformation of NDQ peptides has more conformational freedom than the PPII-like structure of DQ peptides. In addition, it is well known that NDQ peptides have much faster aggregation kinetics compared to DQ peptides.[20,21,28] Thus, increased conformational flexibility of the β-strand-like conformation may contribute to the fast aggregation rate of NDQ peptides.

CONCLUSIONS

Here, we use UVRR spectroscopy, CD spectroscopy, and metadynamics simulations to investigate the structures of DQ15, NDQ15, and DQ20. We find that NDQ15 exists in predominately a β-strand-like conformation, while DQ15 and DQ20 exist in predominately a PPII-like conformation. These results are similar to those previously reported for DQ10 and NDQ10.[20]

We compare the CD spectra of DQ10, NDQ10, DQ15, NDQ15, and DQ20. We find that DQ peptides contain a minority population of the collapsed β-strand-like conformer. We show that longer DQ peptides have larger populations of the collapsed β-strand structure. Our metadynamics simulations show that the PPII-like conformation becomes relatively less energetically favorable and that the PPII → β-strand conformational transition becomes relatively more energetically favorable with increasing polyQ length. This indicates that longer polyQ peptides have an increased propensity for the aggregation-prone collapsed β-strand-like conformation compared to the aggregation-resistant PPII-like conformation. Because the β-strand-like conformation is more prone to aggregation, the increased β-strand-like conformational propensity in longer polyQ peptides

DOI: 10.1021/acs.jpcb.9b01433
J. Phys. Chem. B 2019, 123, 4193−4203

may significantly increase the aggregation kinetics of longer polyQ tracts.

We also used CD spectroscopy to investigate the effects of temperature on the structure of NDQ15 and DQ20. We found that increasing temperature decreases the population of the β-strand-like conformations in both NDQ15 and DQ20. However, we observe no changes in the PPII-like content of DQ10−20 peptides with increasing temperature. Metadynamics simulations show that the β-strand-like energy well is broad, allowing for structural freedom, while that of the PPII-like structure is narrow, suggesting a more well-defined structure with less conformational flexibility. Computational work previously showed that increased conformational flexibility promoted aggregation and fibrillization of polyQ peptides.[16,17] Thus, conformational flexibility may play a role in the fast aggregation kinetics of NDQ peptides in β-strand-like conformations.

Overall, our work provides crucial insights into the connection between polyQ peptide length, structure, and aggregation kinetics. We find that the β-strand-like conformation of polyQ has more conformational freedom compared to the PPII-like conformation, which may contribute to the faster aggregation kinetics of the β-strand-like structure. Our work also shows that longer polyQ peptides increasingly prefer the aggregation-prone β-strand-like conformation over the aggregation-resistant PPII-like conformation. This structural preference likely plays a role in increasing the aggregation kinetics of longer polyQ peptides, which is associated with an earlier age of onset for polyQ neurodegenerative diseases.

■ ASSOCIATED CONTENT

Supporting Information

The Supporting Information is available free of charge on the ACS Publications website at DOI: 10.1021/acs.jpcb.9b01433.

Additional information on UVRR spectral fitting, Ψ angle calculations, modeling of DQ15-20 CD spectra, and UVRR modeling of β-strand subpopulations in DQ peptides (PDF)

Coordinate files for the α-helix, β-strand, and PPII collective variables, as well as python scripts used in the metadynamics simulations (ZIP) (PDB) (PDB) (PDB) (PDB) (PDB) (PDB)

■ AUTHOR INFORMATION

Corresponding Author

*E-mail: asher@pitt.edu.

ORCID

Ryan S. Jakubek: 0000-0001-7880-9422

Stephen E. White: 0000-0002-7786-4400

Sanford A. Asher: 0000-0003-1061-8747

Present Address

‖Department of Biochemistry and Molecular Biology, University of Texas Medical Branch, Galveston, Texas 77555-0304, United States (R.J.W.).

Notes

The authors declare no competing financial interest.

■ ACKNOWLEDGMENTS

Funding for this work was provided by the University of Pittsburgh (R.S.J., S.E.W., S.A.A.) and the Defense Threat Reduction Agency HDTRA-09-14-FRCWMD (R.S.J., S.A.A.), and was partially supported by NIH R01 DA027806 (R.J.W.). S.E.W. gratefully acknowledges support through the Molecular Biophysics and Structural Biology NIH Training Grant (T32 GM 088119). The MD simulation computer time was supported by XSEDE MCB060069, and computer equipment was purchased from NSF funds (CHE01126465 and P116Z080180) (R.J.W.).

■ REFERENCES

(1) Orr, H. T.; Zoghbi, H. Y. Trinucleotide Repeat Disorders. *Annu. Rev. Neurosci.* **2007**, *30*, 575−621.

(2) Nagai, Y.; Inui, T.; Popiel, H. A.; Fujikake, N.; Hasegawa, K.; Urade, Y.; Goto, Y.; Naiki, H.; Toda, T. A Toxic Monomeric Conformer of the Polyglutamine Protein. *Nat. Struct. Mol. Biol.* **2007**, *14*, 332−340.

(3) Lajoie, P.; Snapp, E. L. Formation and Toxicity of Soluble Polyglutamine Oligomers in Living Cells. *PLoS One* **2010**, *5*, No. e15245.

(4) Yang, W.; Dunlap, J. R.; Andrews, R. B.; Wetzel, R. Aggregated Polyglutamine Peptides Delivered to Nuclei Are Toxic to Mammalian Cells. *Hum. Mol. Genet.* **2002**, *11*, 2905−2917.

(5) Liu, K.-Y.; Shyu, Y.-C.; Barbaro, B. A.; Lin, Y.-T.; Chern, Y.; Thompson, L. M.; James Shen, C.-K.; Marsh, J. L. Disruption of the Nuclear Membrane by Perinuclear Inclusions of Mutant Huntingtin Causes Cell-Cycle Re-Entry and Striatal Cell Death in Mouse and Cell Models of Huntington's Disease. *Hum. Mol. Genet.* **2014**, *24*, 1602−1616.

(6) Chen, S.; Ferrone, F. A.; Wetzel, R. Huntington's Disease Age-of-Onset Linked to Polyglutamine Aggregation Nucleation. *Proc. Natl. Acad. Sci.* **2002**, *99*, 11884−11889.

(7) Myers, R. H. Huntington's Disease Genetics. *NeuroRx* **2004**, *1*, 255−262.

(8) Penney, J. B.; Vonsattel, J.-P.; Macdonald, M. E.; Gusella, J. F.; Myers, R. H. CAG Repeat Number Governs the Development Rate of Pathology in Huntington's Disease. *Ann. Neurol.* **1997**, *41*, 689−692.

(9) Chen, S.; Berthelier, V.; Yang, W.; Wetzel, R. Polyglutamine Aggregation Behavior in Vitro Supports a Recruitment Mechanism of Cytotoxicity. *J. Mol. Biol.* **2001**, *311*, 173−182.

(10) Wetzel, R. Physical Chemistry of Polyglutamine: Intriguing Tales of a Monotonous Sequence. *J. Mol. Biol.* **2012**, *421*, 466−490.

(11) Klein, F. A. C.; Pastore, A.; Masino, L.; Zeder-Lutz, G.; Nierengarten, H.; Oulad-Abdelghani, M.; Altschuh, D.; Mandel, J.-L.; Trottier, Y. Pathogenic and Non-Pathogenic Polyglutamine Tracts Have Similar Structural Properties: Towards a Length-Dependent Toxicity Gradient. *J. Mol. Biol.* **2007**, *371*, 235−244.

(12) Chen, S.; Berthelier, V.; Hamilton, J. B.; O'Nuallain, B.; Wetzel, R. Amyloid-like Features of Polyglutamine Aggregates and Their Assembly Kinetics. *Biochemistry* **2002**, *41*, 7391−7399.

(13) Altschuler, E. L.; Hud, N. V.; Mazrimas, J.; Rupp, B. Random Coil Conformation for Extended Polyglutamine Stretches in Aqueous Soluble Monomeric Peptides. *J. Pept. Res.* **1997**, *50*, 73−75.

(14) Nakano, M.; Watanabe, H.; Rothstein, S. M.; Tanaka, S. Comparative Characterization of Short Monomeric Polyglutamine Peptides by Replica Exchange Molecular Dynamics Simulation. *J. Phys. Chem. B* **2010**, *114*, 7056−7061.

(15) Vitalis, A.; Lyle, N.; Pappu, R. V. Thermodynamics of β-Sheet Formation in Polyglutamine. *Biophys. J.* **2009**, *97*, 303−311.

(16) Vitalis, A.; Wang, X.; Pappu, R. V. Atomistic Simulations of the Effects of Polyglutamine Chain Length and Solvent Quality on Conformational Equilibria and Spontaneous Homodimerization. *J. Mol. Biol.* **2008**, *384*, 279−297.

(17) Wang, X.; Vitalis, A.; Wyczalkowski, M. A.; Pappu, R. V. Characterizing the Conformational Ensemble of Monomeric Polyglutamine. *Proteins* **2006**, *63*, 297−311.

(18) Chellgren, B. W.; Miller, A.-F.; Creamer, T. P. Evidence for Polyproline II Helical Structure in Short Polyglutamine Tracts. *J. Mol. Biol.* **2006**, *361*, 362−371.

(19) Bhattacharyya, A.; Thakur, A. K.; Chellgren, V. M.; Thiagarajan, G.; Williams, A. D.; Chellgren, B. W.; Creamer, T. P.; Wetzel, R.

DOI: 10.1021/acs.jpcb.9b01433
J. Phys. Chem. B 2019, 123, 4193−4203

Oligoproline Effects on Polyglutamine Conformation and Aggregation. *J. Mol. Biol.* **2006**, *355*, 524−535.
(20) Punihaole, D.; Jakubek, R. S.; Workman, R. J.; Marbella, L. E.; Campbell, P.; Madura, J. D.; Asher, S. A. Monomeric Polyglutamine Structures That Evolve into Fibrils. *J. Phys. Chem. B* **2017**, *121*, 5953−5967.
(21) Punihaole, D.; Workman, R. J.; Hong, Z.; Madura, J. D.; Asher, S. A. Polyglutamine Fibrils: New Insights into Antiparallel β-Sheet Conformational Preference and Side Chain Structure. *J. Phys. Chem. B* **2016**, *120*, 3012−3026.
(22) Jakubek, R. S.; White, S. E.; Asher, S. A. UV Resonance Raman Structural Characterization of an (In)Soluble Polyglutamine Peptide. *J. Phys. Chem. B.* **2019**, *123*, 1749−1763.
(23) Punihaole, D.; Jakubek, R. S.; Workman, R. J.; Asher, S. A. Interaction Enthalpy of Side Chain Backbone Amides in Polyglutamine Solution Monomers and Fibrils. *J. Phys. Chem. Lett.* **2018**, *9*, 1944−1950.
(24) Jakubek, R. S.; Handen, J.; White, S. E.; Asher, S. A.; Lednev, I. K. Ultraviolet Resonance Raman Spectroscopic Markers for Protein Structure and Dynamics. *TrAC.* **2018**, *103*, 223−229.
(25) Oladepo, S. A.; Xiong, K.; Hong, Z.; Asher, S. A.; Handen, J.; Lednev, I. K. UV Resonance Raman Investigations of Peptide and Protein Structure and Dynamics. *Chem. Rev.* **2012**, *112*, 2604−2628.
(26) Dudik, J. M.; Johnson, C. R.; Asher, S. A. UV Resonance Raman Studies of Acetone, Acetamide, and N-Methylacetamide: Models for the Peptide Bond. *J. Phys. Chem.* **1985**, *89*, 3805−3814.
(27) Xiong, K.; Punihaole, D.; Asher, S. A. UV Resonance Raman Spectroscopy Monitors Polyglutamine Backbone and Side Chain Hydrogen Bonding and Fibrillization. *Biochemistry* **2012**, *51*, 5822−5830.
(28) Chen, S.; Wetzel, R. Solubilization and Disaggregation of Polyglutamine Peptides. *Protein Sci.* **2001**, *10*, 887−891.
(29) Bykov, S.; Lednev, I.; Ianoul, A.; Mikhonin, A.; Munro, C.; Asher, S. A. Steady-State and Transient Ultraviolet Resonance Raman Spectrometer for the 193–270 nm Spectral Region. *Appl. Spectrosc.* **2005**, *59*, 1541−1552.
(30) Jorgensen, W. L.; Chandrasekhar, J.; Madura, J. D.; Impey, R. W.; Klein, M. L. Comparison of Simple Potential Functions for Simulating Liquid Water. *J. Chem. Phys.* **1983**, *79*, 926−935.
(31) Phillips, J. C.; Braun, R.; Wang, W.; Gumbart, J.; Tajkhorshid, E.; Villa, E.; Chipot, C.; Skeel, R. D.; Kale, L.; Schulten, K. Scalable Molecular Dynamics with NAMD. *J. Comput. Chem.* **2005**, *26*, 1781−1802.
(32) Humphrey, W.; Dalke, A.; Schulten, K. VMD: Visual Molecular Dynamics. *J. Mol. Graph.* **1996**, *14*, 33−38.
(33) Huang, J.; MacKerell, A. D. CHARMM36 All-Atom Additive Protein Force Field: Validation Based on Comparison to NMR Data. *J. Comput. Chem.* **2013**, *34*, 2135−2145.
(34) Darden, T.; York, D.; Pedersen, L. Particle Mesh Ewald: An N Log (N) Method for Ewald Sums in Large Systems. *J. Chem. Phys.* **1993**, *98*, 10089−10092.
(35) Martyna, G. J.; Tobias, D. J.; Klein, M. L. Constant Pressure Molecular Dynamics Algorithms. *J. Chem. Phys.* **1994**, *101*, 4177−4189.
(36) Barducci, A.; Bussi, G.; Parrinello, M. Well-Tempered Metadynamics: A Smoothly Converging and Tunable Free-Energy Method. *Phys. Rev. Lett.* **2008**, *100*, No. 020603.
(37) Laio, A.; Parrinello, M. Escaping Free-Energy Minima. *Proc. Natl. Acad. Sci. USA* **2002**, *99*, 12562−12566.
(38) *Molecular Operating Environment (MOE), 2013.08*; Chemical Computing Group Inc.: Montreal, QC, 2016.
(39) Laio, A.; Rodriguez-Fortea, A.; Gervasio, F. L.; Ceccarelli, M.; Parrinello, M. Assessing the Accuracy of Metadynamics. *J. Phys. Chem. B* **2005**, *109*, 6714−6721.
(40) Punihaole, D.; Hong, Z.; Jakubek, R. S.; Dahlburg, E. M.; Geib, S.; Asher, S. A. Glutamine and Asparagine Side Chain Hyperconjugation-Induced Structurally Sensitive Vibrations. *J. Phys. Chem. B* **2015**, *119*, 13039−13051.
(41) Punihaole, D.; Jakubek, R. S.; Dahlburg, E. M.; Hong, Z.; Myshakina, N. S.; Geib, S.; Asher, S. A. UV Resonance Raman Investigation of the Aqueous Solvation Dependence of Primary Amide Vibrations. *J. Phys. Chem. B* **2015**, *119*, 3931−3939.
(42) Asher, S. A.; Ianoul, A.; Mix, G.; Boyden, M. N.; Karnoup, A.; Diem, M.; Schweitzer-Stenner, R. Dihedral Psi Angle Dependence of the Amide III Vibration: A Uniquely Sensitive UV Resonance Raman Secondary Structural Probe. *J. Am. Chem. Soc.* **2001**, *123*, 11775−11781.
(43) Mikhonin, A. V.; Bykov, S. V.; Myshakina, N. S.; Asher, S. A. Peptide Secondary Structure Folding Reaction Coordinate: Correlation Between UV Raman Amide III Frequency, Psi Ramachandran Angle, and Hydrogen Bonding. *J. Phys. Chem. B* **2006**, *110*, 1928−1943.
(44) Asher, S. A.; Mikhonin, A. V.; Bykov, S. UV Raman Demonstrates That α-Helical Polyalanine Peptides Melt to Polyproline II Conformations. *J. Am. Chem. Soc.* **2004**, *126*, 8433−8440.
(45) Xiong, K.; Ma, L.; Asher, S. A. Conformation of Poly-L-Glutamate Is Independent of Ionic Strength. *Biophys. Chem.* **2012**, *162*, 1−5.
(46) Ma, L.; Hong, Z.; Sharma, B.; Asher, S. UV Resonance Raman Studies of the NaClO4 Dependence of Poly-l-Lysine Conformation and Hydrogen Exchange Kinetics. *J. Phys. Chem. B* **2012**, *116*, 1134−1142.
(47) Hovmöller, S.; Zhou, T.; Ohlson, T. Conformations of Amino Acids in Proteins. *Acta Crystallogr., Sect. D: Biol. Crystallogr.* **2002**, *58*, 768−776.
(48) Krimm, S.; Mark, J. E. Conformations of Polypeptides with Ionized Side Chains of Equal Length. *Proc. Natl. Acad. Sci. USA* **1968**, *60*, 1122−1129.
(49) Mikhonin, A. V.; Myshakina, N. S.; Bykov, S. V.; Asher, S. A. UV Resonance Raman Determination of Polyproline II, Extended 2.5_1-Helix, and β-Sheet Ψ Angle Energy Landscape in Poly-L-Lysine and Poly-L-Glutamic Acid. *J. Am. Chem. Soc.* **2005**, *127*, 7712−7720.
(50) Jha, A. K.; Colubri, A.; Zaman, M. H.; Koide, S.; Sosnick, T. R.; Freed, K. F. Helix, Sheet, and Polyproline II Frequencies and Strong Nearest Neighbor Effects in a Restricted Coil Library. *Biochemistry* **2005**, *44*, 9691−9702.
(51) Feng, L. *Molecular Dynamics Predicts The Solution Conformations of Poly-L-Lysine in Salt Solutions*; University of Pittsburgh, 2014.
(52) Buck, M.; Bouguet-Bonnet, S.; Pastor, R. W.; MacKerell, A. D. Importance of the CMAP Correction to the CHARMM22 Protein Force Field: Dynamics of Hen Lysozyme. *Biophys. J.* **2006**, *90*, L36−L38.
(53) Woody, R. W. Theory of Circular Dichroism of Proteins. *Circular Dichroism and the Conformational Analysis of Biomolecules*; Fasman, G. D., Ed.; Plenum Press: New York, 1996; pp 25−67.
(54) Walters, R. H.; Murphy, R. M. Examining Polyglutamine Peptide Length: A Connection between Collapsed Conformations and Increased Aggregation. *J. Mol. Biol.* **2009**, *393*, 978−992.
(55) Sreerama, N.; Woody, R. W. Molecular Dynamics Simulations of Polypeptide Conformations in Water: A Comparison of α, β, and Poly (pro) II Conformations. *Proteins: Struct., Funct., Bioinf.* **1999**, *36*, 400−406.
(56) Adzhubei, A. A.; Sternberg, M. J. E. Left-Handed Polyproline II Helices Commonly Occur in Globular Proteins. *J. Mol. Biol.* **1993**, *229*, 472−493.
(57) Mezei, M.; Fleming, P. J.; Srinivasan, R.; Rose, G. D. Polyproline II Helix Is the Preferred Conformation for Unfolded Polyalanine in Water. *Proteins: Struct., Funct., Bioinf.* **2004**, *55*, 502−507.
(58) Drozdov, A. N.; Grossfield, A.; Pappu, R. V. Role of Solvent in Determining Conformational Preferences of Alanine Dipeptide in Water. *J. Am. Chem. Soc.* **2004**, *126*, 2574−2581.
(59) Fleming, P. J.; Fitzkee, N. C.; Mezei, M.; Srinivasan, R.; Rose, G. D. A Novel Method Reveals That Solvent Water Favors Polyproline II over β-Strand Conformation in Peptides and Unfolded Proteins: Conditional Hydrophobic Accessible Surface Area (CHASA). *Protein Sci.* **2005**, *14*, 111−118.
(60) Horton, H. R.; Moran, L. A.; Ochs, R. S.; Rawn, J. D.; Scrimgeour, K. G. *Principles of Biochemistry*; Prentice Hall: Upper Saddle River, NJ, 1996.

DOI: 10.1021/acs.jpcb.9b01433
J. Phys. Chem. B 2019, 123, 4193−4203

(61) Darnell, G.; Orgel, J. P. R. O.; Pahl, R.; Meredith, S. C. Flanking Polyproline Sequences Inhibit β-Sheet Structure in Polyglutamine Segments by Inducing PPII-like Helix Structure. *J. Mol. Biol.* **2007**, *374*, 688−704.

DOI: 10.1021/acs.jpcb.9b01433
J. Phys. Chem. B 2019, 123, 4193−4203